[American Journal of Science, Vol. 310, October, 2010, P. 753–773, DOI 10.2475/08.2010.03]

# DYNAMICS OF AN ALPINE CIRQUE GLACIER

J. W. SANDERS*, K. M. CUFFEY**,*, K. R. MACGREGOR***, J. L. KAVANAUGH[§], and C. F. DOW[§§]

**ABSTRACT. Alpine cirques are excavated by glacial erosion, a process that depends in turn on the movement of ice by basal sliding. Cirque glacier flow is usually depicted as rotational sliding of a rigid block, but this model is based on little evidence and implies unorthodox glacier behavior given typical cirque dimensions. The small (~1 km$^2$), temperate West Washmawapta Glacier occupies an archetypal overdeepened and "armchair-shaped" cirque in the Canadian Rockies. We measured (1) the annual surface velocity field, (2) ice thickness, (3) sliding and internal deformation at one borehole, and (4) sliding in a marginal cavity. The glacier moves slowly, with surface velocities of 3 to 10 m/yr. The maximum ice thickness (~185 m) occurs in the center of the cirque basin and roughly coincides with the position of greatest ice flux. Using our field measurements, a standard constitutive relation for ice, and simplifying assumptions related to the depth distribution of strain rates, we approximated the driving and resisting forces acting on sections of the glacier, and inferred the general pattern of basal sliding. Sliding is minimum in the center of the cirque and increases toward the margins, especially up the stoss side of the riegel. Internal deformation accounts for all motion in the cirque center, even if an unusually low viscosity for temperate ice is assumed. Basal shear stresses tend toward $10^5$ Pa everywhere, a typical value for mountain glaciers. Transverse and longitudinal straining are significant in some parts of the glacier. Although a component of rotational flow must occur internally, the glacier does not conform to the rotational sliding model in any essential respect.**

## INTRODUCTION

Glaciers in mountainous terrain excavate cirques at the heads of valleys and in recesses along major ridgelines. Cirque distribution and morphology profoundly influence the topography near drainage divides, a fact recognized long ago (Gastaldi, 1873; Helland, 1877; Matthes, 1900; Richter, 1900; Johnson, 1904; Lawson, 1904; Daly, 1905; Penck, 1905; Davis, 1906). Willard Johnson (1904) famously described the imprint of cirques: "I likened the [summit upland] to the irregular remnants of a sheet of dough, on the biscuit board, after the biscuit tin has done its work." Modern investigators emphasize that cirques affect the relief structure, hypsometry, and distribution of slopes (for example, Mitchell and Montgomery, 2006). A recent renewal of interest in cirques has emerged from efforts to disentangle the roles of glacial and fluvial erosion in the topographic evolution of the cores of mountain ranges (Brocklehurst and Whipple, 2002; Oskin and Burbank, 2005; Brook and others, 2006; Mitchell and Montgomery, 2006; Naylor and Gabet, 2007; Foster and others, 2008). In this context, it is essential to develop a process-based understanding of cirque development. Such a model, in turn, requires an accurate view of the dynamical behavior of glaciers occupying cirques (Weertman, 1971; Hooke, 1991; MacGregor and others, 2009).

* Department of Earth and Planetary Science, 307 McCone Hall, University of California, Berkeley, California, 94720, USA; jws@eps.berkeley.edu
** Department of Geography, 507 McCone Hall, University of California, Berkeley, California, 94720, USA; kcuffey@berkeley.edu
*** Geology Department, Macalester College, St. Paul, Minnesota, 55105, USA
§ Department of Earth and Atmospheric Sciences, University of Alberta, Edmonton, Alberta T6G 2E3, Canada
§§ Department of Geography, University of Wales—Swansea, Singleton Park, Swansea, SA2 8PP, United Kingdom

At present, the prevailing model of cirque glacier flow depicts a nearly rigid, rotating block that slides along an arcuate bed (Summerfield, 1991; Evans, 1997 and 2006; Ritter and others, 2002). One popular text states, for example, that ". . . [cirque] glaciers move by a process known as rotational sliding, in which the ice slides over the arcuate bedrock floor, rotating at the same time around a horizontal axis." (Ritter and others, 2002, p. 329). This picture originated in the classic study by W. V. Lewis and colleagues of a small cirque glacier in Norway (Clark and Lewis, 1951; McCall, 1952 and 1960; Lewis, 1960), a study that drew on earlier work in Montana by Gibson and Dyson (1939). The investigators in Norway dug an englacial tunnel, which exposed dipping ablation surfaces. Waldrop (1964) made similar observations of ablation surfaces and attributed the dip pattern to rotational sliding. Rotational sliding is an appealing model because it offers a simple explanation for cirque formation: the basin develops as ice revolves about a central, horizontal pivot (akin to a scoop in a tub of ice cream). Although a specialist in ice dynamics might regard the rigid-rotation model with skepticism, the rotational sliding paradigm is nonetheless entrenched in the cirque literature and no critical investigations of cirque-glacier flow have been made for more than 50 years. Our study begins to fill this void.

Although a component of rotational flow will occur anytime that ice slides on a curved bed, a glacier-wide dominance of rotational sliding would be unusual. A typical alpine cirque basin is of order 1 km in length, while the occupying glacier should normally have a depth of order 0.1 km; thus, even cirque glaciers tend to be considerably longer than they are deep, a geometry that inherently limits the importance of rotational motion. Regardless of the geometry, rigid motion occurs only if deviatoric stresses remain well below the effective plastic strength of ice, about $10^5$ Pa, a situation that normally only occurs if the bed is exceptionally slippery or the glacier is stagnating. Furthermore, upglacier dips of ablation surfaces are not diagnostic of the mechanism of motion; they are expected whether or not the ice slides. Specifically, internal deformation of mountain glaciers usually involves a component of downward flow in the accumulation zone and upward flow in the ablation zone, a consequence of longitudinal extension and compression related to the systematic downglacier variation of ice flux. Thus a rotation and tilting of layers normally occurs even in the absence of sliding. It follows that rigid rotation is not necessary to explain the original findings of McCall (1952) and (1960). Surface velocity vectors at Vesl-Skautbreen indicate that the glacier is in a state of longitudinal compression over its entire length (see fig. 2 of McCall, 1952). Consequently, the upglacier dip of annual bands will increase progressively during transport toward the front margin.

Here we report the first findings from a new study of a cirque glacier in the Rocky Mountains of Canada. Our report seeks to illuminate the essential behavior of a glacier that still occupies its entire cirque basin, by addressing several questions: How does the velocity field of a cirque glacier vary across the surface? What percentage of the total motion results from basal slip? What are the magnitude and spatial distribution of forces driving and retarding glacier flow? We measured ice thicknesses and surface velocity vectors over most of the glacier, and calculated the vertically-integrated balance of forces at several locations. We also measured internal deformation in one borehole.

## SITE DESCRIPTION AND ICE THICKNESS SURVEY

Our study site is the east-facing cirque of Helmet Mountain, a prominent horn-type summit (3124 m) in the Vermilion Range of British Columbia (figs. 1 and 2). The cirque is carved in Cambrian-age calcareous slate and argillaceous limestone and dolomite, cross-cut by thin dikes of Devonian age (Cook, 1975). In elevation and dimensions, our study site resembles many other cirques in the Rocky Mountains (McLaren and Hills, 1973; Graf, 1976; Trenhaile, 1976).

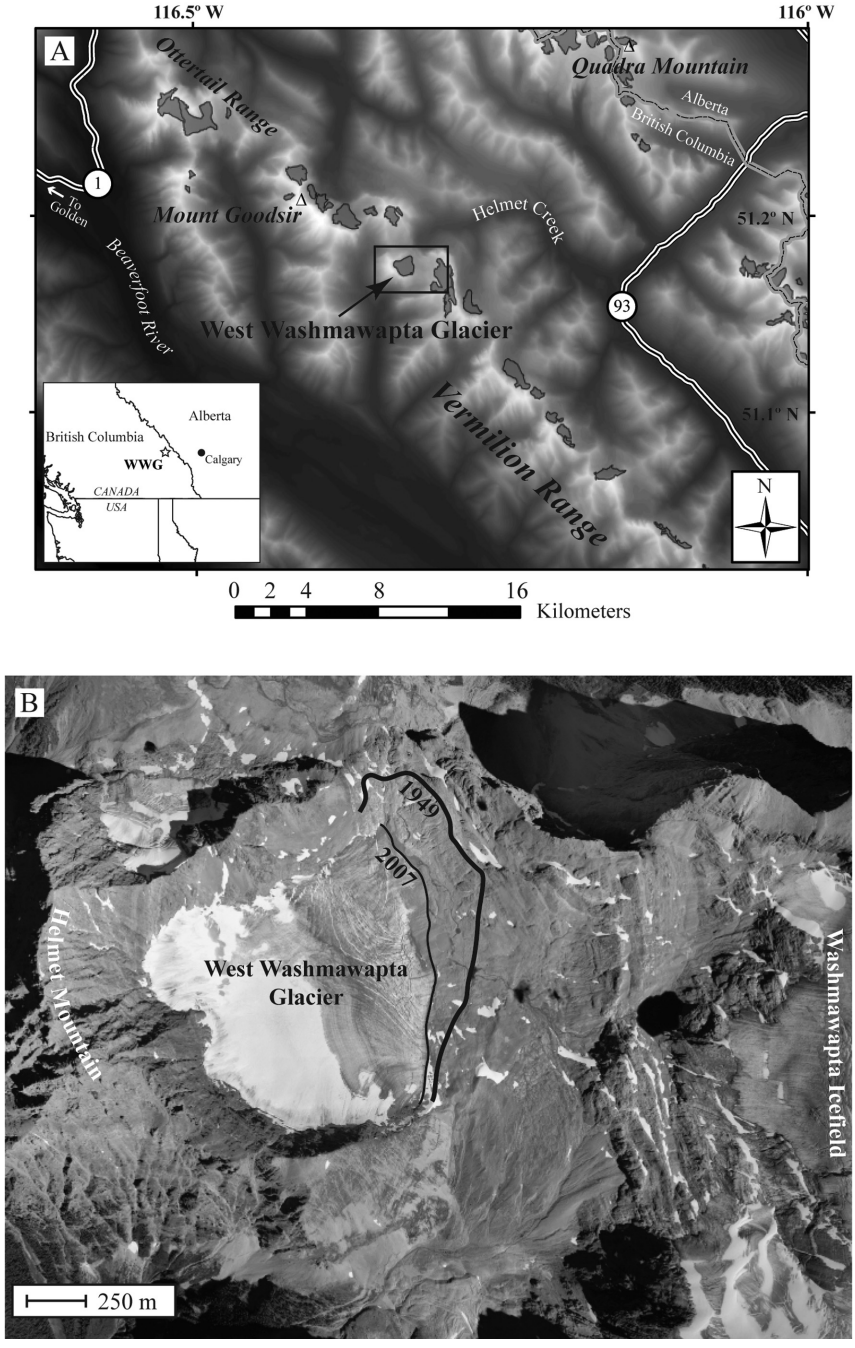


Fig. 1. (A) Location map showing the broader geographic and topographic context of West Washmawapta Glacier (other nearby glaciers are shown in solid gray). (B) Aerial photograph of West Washmawapta Glacier (WWG) taken August 15, 2007. As recently as 1949 (the oldest aerial photograph we obtained), WWG and the Washmawapta Icefield still abutted one another.

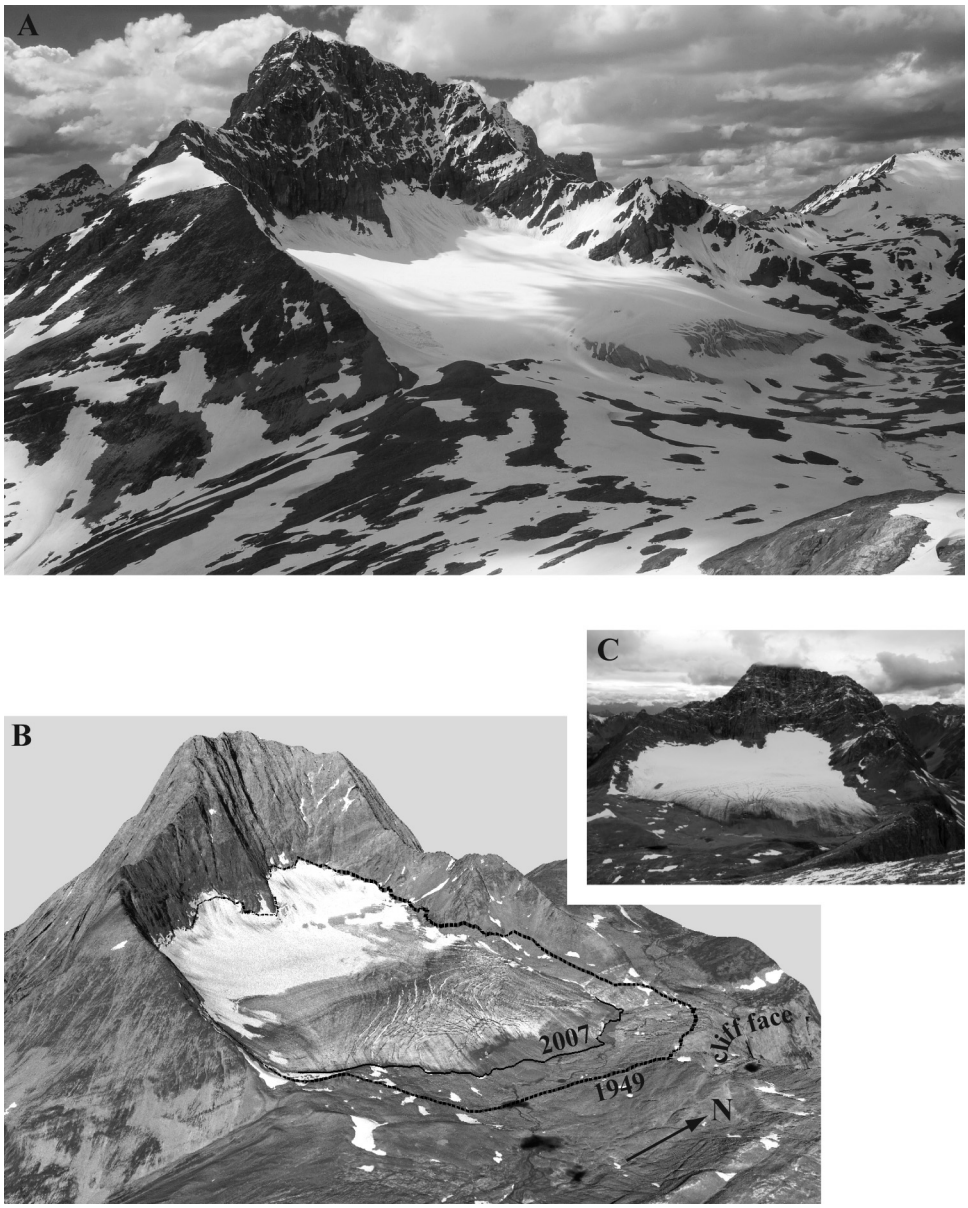


Fig. 2. (A) West Washmawapta Glacier and Helmet Mountain in June, 2007 (view looking northwest). Steep avalanche aprons and gently-sloping central plain are both evident in the photo. (B) Drawing the 1949 glacier boundary (fig. 1B) on a digital elevation model image illustrates recent retreat and thinning of the glacier. Expansion of WWG is limited by a cliff to the northeast and the Washmawapta Icefield to the east. (C) Head-on view of WWG in August, 2008.

Occupying the cirque is West Washmawapta Glacier (WWG), western remnant of the formerly continuous Washmawapta Icefield (figs. 1B and 2). During the peak Cavell Advance (Little Ice Age), ice emerged from the cirque, flowed across a proglacial plateau, and then descended over the brink of a cliff (Luckman and Osborn, 1979). Subsequent retreat shrank the glacier considerably, including a 30 percent

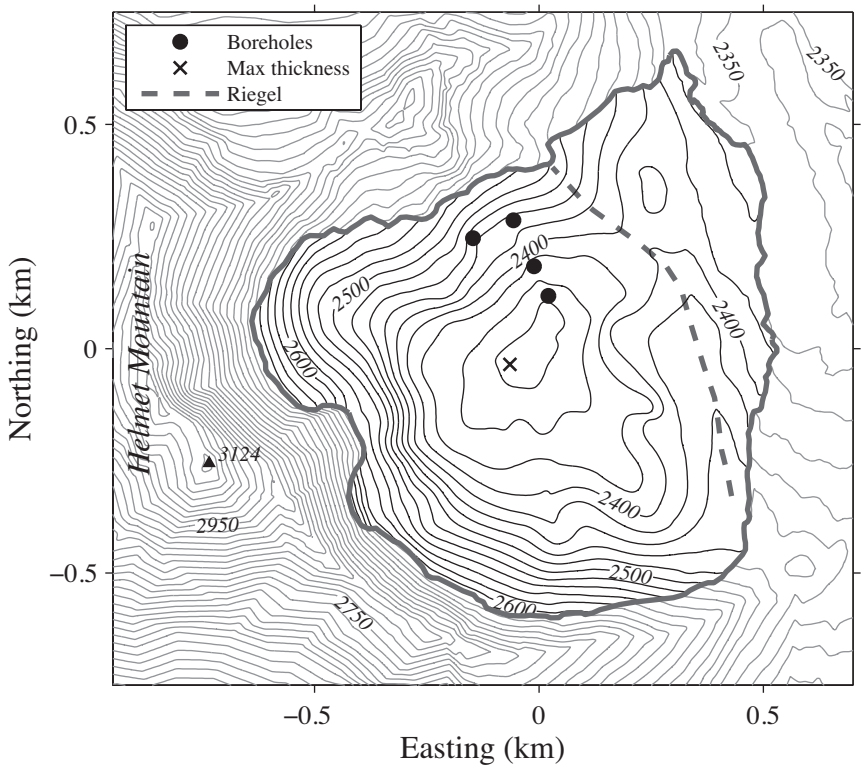


Fig. 3. Topographic map of Helmet Mountain Cirque showing subglacial topography (contour interval: 20 m). Six boreholes (located at black circles) provided a check on our ice thickness map (overlapping symbols are shown as one). The local grid is referenced to 51.1773° N, 116.3296° W in this and all subsequent plan-view figures.

reduction between 1949 and 2007 (figs. 1B and 2B). Currently, WWG covers an area of about one square kilometer and continues to retreat. It flows over a riegel at the outer edge of its cirque basin, and terminates on the riegel's downvalley slope (figs. 3 and 4). The glacier and surrounding cirque walls resemble a reclined armchair, with steep head and toe sections connected by a flatter central expanse (fig. 2B). In the middle and southern parts of the glacier, the equilibrium line is positioned approximately over the center of the cirque basin (as indicated by the late summer snowline seen in figs. 4 and 5). In the northern part, the ablation zone is more extensive and the equilibrium line shifts westward toward the headwall (fig. 5). This pattern should be contrasted with a glacier that originates in a cirque but flows far down-valley; in such a glacier, the cirque lies entirely within the accumulation zone and the dynamics would differ in some respects from the case studied here.

From our own on-site weather station data, cross-correlated with continuous records from the B.C. Ministry of Environment's Floe Lake monitoring site (about 20 km distant), we estimated a mean annual temperature at WWG of −2.4°C for the period 1/2004 through 12/2007. Summers are warm, and abundant surface melt permeates the firn. The glacier is therefore temperate—a conclusion verified by direct measurements of temperature in moulins and boreholes, and by observations of abundant unfrozen water within the glacier (Dow, ms, 2009).

To map the thickness of the glacier, we used an Icefield Instruments™ ice-penetrating radar system with a 5 MHz center frequency and 10 m antennae set 50 m

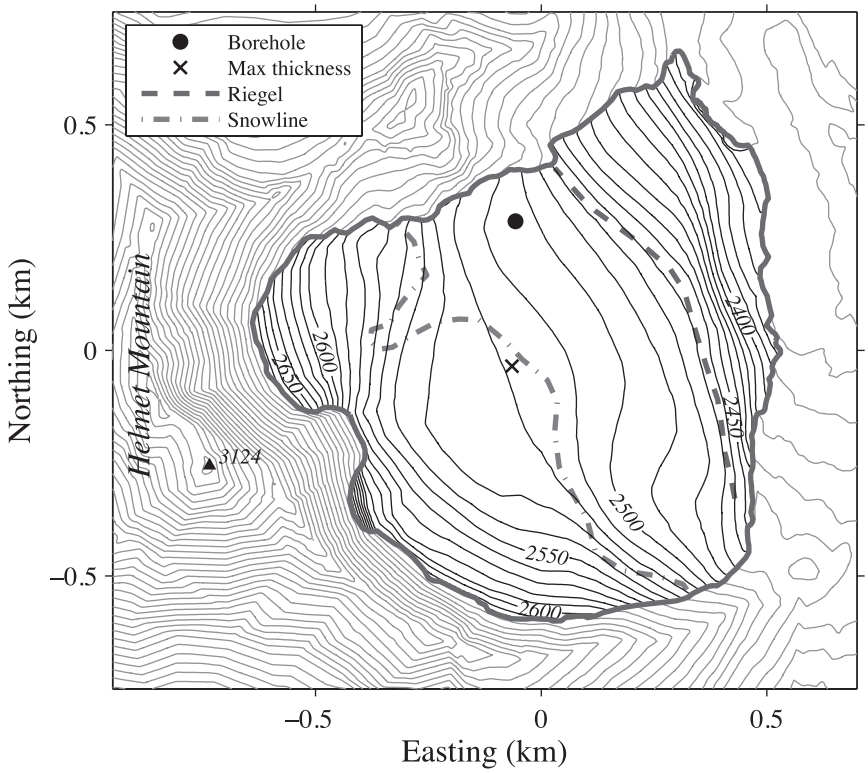


Fig. 4. West Washmawapta Glacier ice surface (black contours, contour interval: 10 m) and the surrounding cirque (gray contours, contour interval: 20 m). Ice flow is predominantly left to right. Maximum ice thickness (~185 m) is found in the center of the overdeepening (black x). Elevations were photogrammetrically derived from aerial images acquired 8/05/2006 by Fotoflight, Inc. (Calgary, AB) and processed by HJW Geospatial, Inc. (Oakland, CA).

apart. The system was deployed along 10 longitudinal and 11 transverse profiles. The reflections, recorded on a Fluke 199C Scopemeter™, were post-processed by removing high-frequency noise, amplifying the remaining signal as a function of depth, assuming a signal propagation speed of $1.68 \times 10^8$ m/s, and migrating individual profiles using the circle-tangent technique. Comparison with the depths of six boreholes drilled through the glacier (using a hot-water system) showed that the thickness map obtained by radar was generally accurate to better than 10 percent of the ice depth ($7 \pm 4$ m). Near the steeply-sloping marginal walls, however, where the ice is thin and the topography complex, errors increased to $13 \pm 2$ m ($27 \pm 8\%$).

The survey revealed an average glacier depth of about 70 m, and maximum depth of about 185 m. A map of bedrock topography was derived by subtracting ice thicknesses from a photogrammetrically-derived digital elevation model of the surface (figs. 3 and 4). The glacier occupies a cirque basin "overdeepening" of archetypal form; continued retreat of the glacier would leave a deep lake between the headwall and riegel.

### ice flux and surface velocities

We measured the surface motion of WWG using repeat differential GPS surveys of 89 metal and/or PVC poles emplaced 2 to 3 meters in the ice. The surveys were

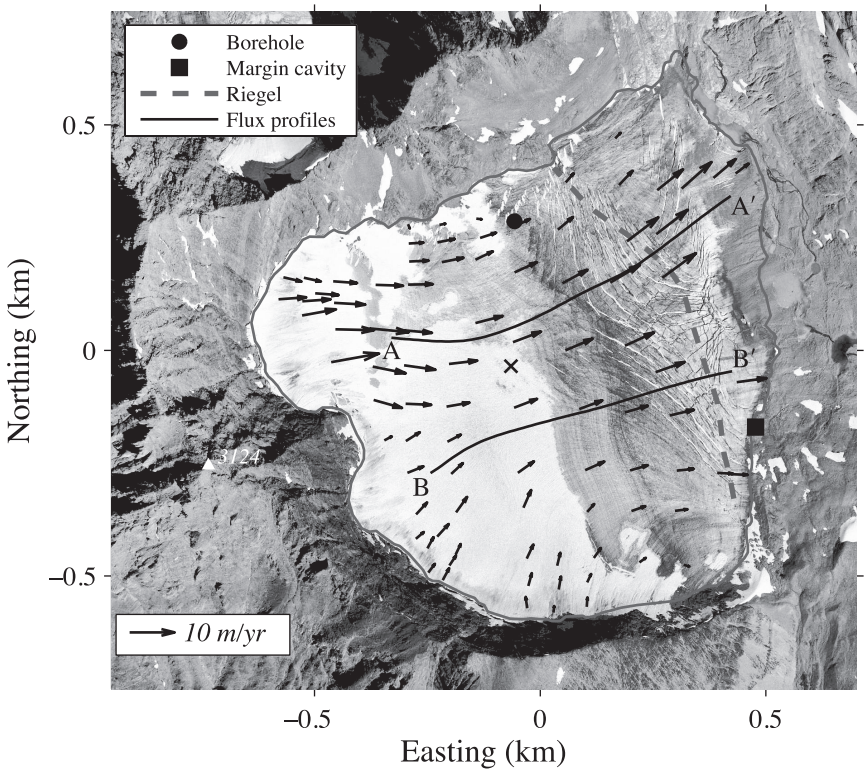


Fig. 5. Composite horizontal surface velocity field of West Washmawapta Glacier (superimposed on an aerial photograph taken 8/15/2007). Lengths of velocity vectors indicate 10 years of displacement at the measured annual rates.

referenced to two continuously-running base stations on separate bedrock knobs in the glacier foreland, located within 350 m of the ice margin. Surveys were made during three consecutive summer field seasons (2006–2008), and incorporated 53 survey markers that survived the first full winter. Velocities in different field seasons and different periods within field seasons were strongly correlated, indicating that the spatial pattern of flow changed little over time (correlation coefficients for velocities at the same location but measured in different periods averaged 0.94 ± 0.03). Formal GPS-positioning error magnitudes never exceeded 10 mm, except at stakes located within about 100 m of the headwall. Other survey errors, primarily the result of leaning or bent stakes, are harder to quantify. Close inspection of velocities at individual poles, however, revealed random, uncorrelated temporal velocity variations that can only be explained by survey errors. In the end, this random component of our surveyed velocities suggests errors of about 0.2 to 0.3 m/yr, or roughly 5 percent of the annual motion. In the second field season, having determined that the spatial pattern of flow did not change significantly, we reduced the number of survey poles in the original grid and installed additional poles across the front margin.

Figure 5 shows the spatial pattern of horizontal velocities on the glacier surface. The glacier moves slowly, at 3 to 10 m/yr. Ice and firn flow away from both the southern and western headwalls, where avalanche and wind deposition of snow cause rapid accumulation that builds a steep surface apron. Ice originating along the southern flank turns 90 degrees eastward to cross the riegel. In the northeastern

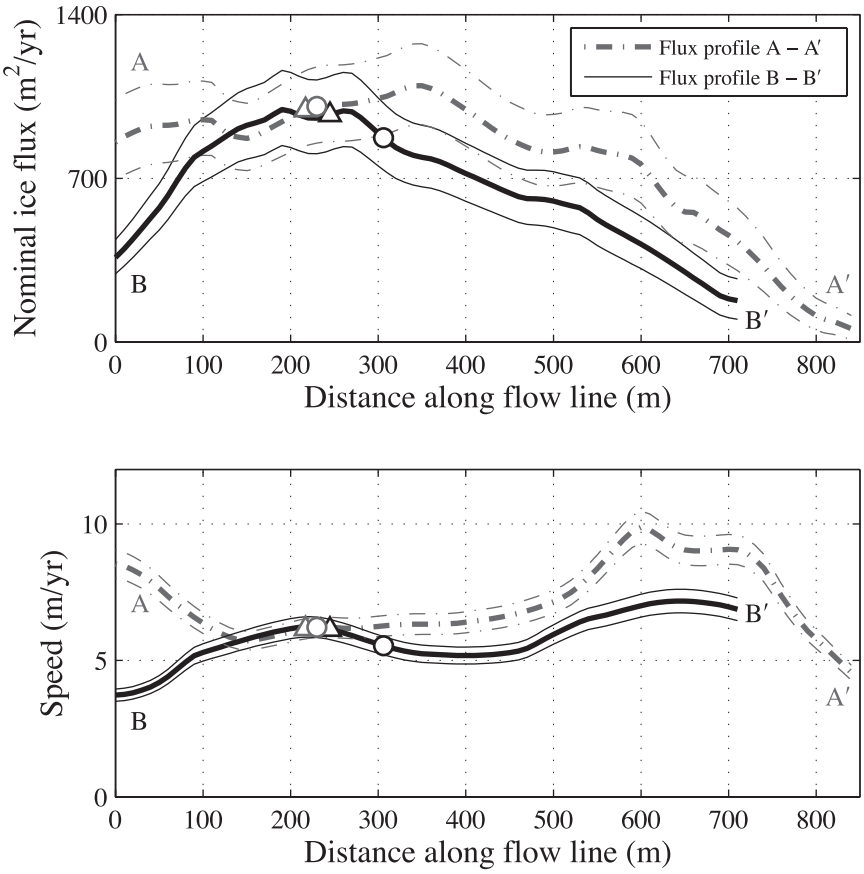


Fig. 6. (A) Nominal ice flux magnitudes (per unit width across-glacier) along profiles A–A′ and B–B′, with error bounds indicated by thin lines. Triangles and circles denote the point each flux line crosses the equilibrium line, inferred from elevation contours and the contemporary late-summer snowline, respectively. Both equilibrium line proxies match well with peak ice fluxes. (B) Surface speed along the same profiles.

quadrant, a partial breach of the riegel steers and concentrates the flow. Transverse shearing is most important along the northern margin, but also occurs along the southeastern margin and the western part of the flowline that crosses the glacier's center.

Figure 6 displays the variation of nominal ice flux (per unit width across-glacier) and surface speed along two flowlines. Here "nominal flux" equals the product of surface speed and ice thickness, a quantity that for glaciers is usually within 20 percent of the true ice flux (Cuffey and Paterson, 2010, p. 310). The nominal flux along both flowlines reaches a maximum whose position roughly corresponds to the equilibrium line, inferred from ice surface contours and observations of the snowline at the end of each summer. Along the northern flowline, the extensive zone with little change of flux is consistent with observations of patchy firn in this region (fig. 5).

### FORCE BALANCE AND PATTERN OF SLIDING

The erosion rate beneath glaciers is expected to increase with the rate of basal sliding (Hallet, 1979 and 1996). However, direct measurements of basal sliding are

usually difficult to make. Alternatively, basal sliding can be inferred as the residual of the velocity at the surface of the glacier ($u_s$) minus the contribution from internal deformation ($u_d$)

$$u_b = u_s - u_d \tag{1}$$

where $u_b$ denotes the basal sliding rate. To approximate the deformational velocity, it is common to assume that the force driving flow is resisted solely by the basal drag, $\tau_b$. Per unit area of glacier, the driving force is referred to as driving stress, denoted $\tau_d$, and calculated as the product of ice thickness, surface slope, and unit weight of ice. Setting $\tau_d = \tau_b$ gives the classic formula for a slab glacier (Nye, 1952). Integrating over the ice thickness, $H$, and assuming a linear increase of shear stress with depth, gives

$$u_d = \frac{2A}{(n+1)} \tau_b^n H \tag{2}$$

where $A$ is the creep parameter of ice and $n$ can be taken as 3 (Cuffey and Paterson, 2010, p. 55–57). Given a value $A = 1.5 \times 10^{-24}$ Pa$^{-3}$s$^{-1}$ and basal stress of $10^5$ Pa, equation (2) implies a deformational velocity of 2 to 5 m/yr for ice 100 to 200 m thick, respectively. At WWG, because the surface moves at about 5 m/yr where the glacier is 180 m thick, but more rapidly in the thin parts over the riegel and sides, the sliding component must increase away from the thick central basin. Moreover, no sliding is necessary to explain the observed 5 m/yr of flow in the center of the cirque, even if the ice is assumed to be unusually stiff (low value of $A$, see below) for a temperate glacier.

It is also known, however, that the magnitude of driving stress tends to vary spatially more than the basal shear stress, because stress-gradient forces suppress variations of the ice flow (Cuffey and Paterson, 2010, p. 327). In regions of the glacier where the driving stress and basal drag are not equivalent, equation (2) over- or under-estimates the basal sliding rate. A more rigorous approach—that makes no assumptions about the relationship between $\tau_d$ and $\tau_b$—is therefore necessary. To perform such an analysis, we combined surface velocity, ice thickness, and surface elevation data to estimate vertically-integrated forces, which in turn allows for partitioning of ice motion between basal slip and internal shear at several locations on the glacier.

To begin, consider a cylindrical column of ice, with plan-view area $S$, and thickness $H$, extending vertically through the glacier. We calculate the portion of surface velocity arising from internal shear as

$$u_d = \int_0^H \frac{\partial u}{\partial z}\, dz = 2A \int_0^H \tau_E^{n-1} \tau_{xz} dz \tag{3}$$

where $\tau_E$ is the effective stress, and $\tau_{xz}$ is a function of $\tau_b$ (see below). The effective stress magnitude is defined as

$$2\tau_E^2 = \tau_{xx}^2 + \tau_{yy}^2 + \tau_{zz}^2 + 2(\tau_{xz}^2 + \tau_{yz}^2 + \tau_{xy}^2) \tag{4}$$

and, from the definition of deviatoric stress,

$$\tau_{zz} = -(\tau_{xx} + \tau_{yy}) \tag{5}$$

We define coordinates $x$, $y$, and $z$ as downglacier, across-glacier, and upward-vertical, respectively. Here, terms written as $\tau$ with two subscripts denote components of the deviatoric stress tensor (and an arbitrary component will be written $\tau_{ij}$). The downglacier gravitational driving force causing internal shear is

$$\tau_d S = \rho_i g H \alpha S \tag{6}$$

for surface slope $\alpha$, density $\rho_i$, and gravitational acceleration $g$. This force is balanced by resisting forces acting on the base ($\tau_b S$) and sides. (For a thorough explanation of force terms see van der Veen and Whillans, 1989). As a convenient notation, the balance of these forces can be written

$$\tau_d = \tau_b + \tau_l + \tau_w \tag{7}$$

where each term is a force on the cylinder, normalized to surface area (the four terms represent driving stress, basal drag, longitudinal drag, and wall drag, respectively). The objective is to estimate the basal shear stress, $\tau_b$, as the residual $\tau_d - \tau_w - \tau_l$. The longitudinal and wall drags are found by taking the surface integral, around the whole cylinder, of longitudinal resistive stresses ($\tau_{xx} - \tau_{zz} = 2\tau_{xx} + \tau_{yy}$) and transverse shear stresses ($\tau_{xy}$), respectively.

We assume the standard isotropic constitutive relation for ice (the "generalized Glen's Law") to relate strain rate components $\dot{\varepsilon}_{ij}$ to deviatoric stresses

$$\dot{\varepsilon}_{ij} = A \tau_E^{n-1} \tau_{ij} \tag{8}$$

with variables as described above. To derive $\tau_w$ and $\tau_l$, we calculate deviatoric stresses from equation (8) using values for strain rates measured at the surface (from our velocity field) and projected downward.

Several difficulties confront this analysis:

(1) Force balance analyses of this sort—constrained by measurements of surface strain rates and velocities but not by measurements at the bed—are inherently unstable if the fundamental stress-equilibrium equations are used to calculate the variation of strain rate components with depth (Bahr and others, 1994). An approximation strategy must be adopted (Truffer, 2004; Maxwell and others, 2008; Kavanaugh and Cuffey, 2009). We assume, first, a linear variation of $\tau_{xz}$ over depth

$$\tau_{xz} = \tau_b \left(1 - \frac{z}{H}\right) \tag{9}$$

for height above bed $z$ and ice thickness $H$. This assumption is exact when $\tau_w$ and $\tau_l$ are negligible. Second, we specify *a priori* how the strain rates $\dot{\varepsilon}_{xx}$, $\dot{\varepsilon}_{yy}$, and $\dot{\varepsilon}_{xy}$ vary with depth. Their surface values are known from our velocity measurements. Below the surface, we use two different scenarios: 1) constant values over depth and 2) linear decline from the measured value at the surface to zero at the bed. While the strain rates in the upper half of the ice thickness must in general be related to values observed at the surface, we have no similar constraint on strain rates in the bottom half. Note, however, that the stress $\tau_{xz}$ increases with depth and, because of the non-linearity of equation (8) when $n = 3$, $\dot{\varepsilon}_{xz}$ will greatly exceed the other strain rate components and thus dominate the contribution of the lower-half to the vertically-integrated forces.

(2) A second problem is that the non-linearity of ice creep (the power $n = 3$ in eq 8) makes the calculated internal shear sensitive to small variations of ice thickness. Because the uncertainty in our ice thickness values is about 10 percent, the corresponding uncertainty in shear velocity is about 30 percent. Internal shear also depends sensitively on surface slope, but we perform the calculations for large enough regions that errors in surface slope are negligible. By incrementally expanding the radius of the cylindrical region being

Table 1

*Calculated forces and sliding rates for the 12 regions shown in figure 7*

| Region | $H$ | $\alpha$ | $u_d$ | $u_b$ | $\tau_d$ | $\tau_b$ | $-\tau_w$ | $-\tau_l$ |
|---|---|---|---|---|---|---|---|---|
| | (m) | (degrees) | (m/yr) | (m/yr) | ($10^5$ Pa) | ($10^5$ Pa) | ($10^5$ Pa) | ($10^5$ Pa) |
| **1** | 64 | 7.3 | 1.3 | 2.7 | 0.7 | 0.8 | -0.01 | 0.17 |
| **2** | 69 | 8.4 | 1.9 | 2.7 | 0.9 | 1.0 | -0.07 | 0.15 |
| **3** | 146 | 5.4 | 4.7 | 1.6 | 1.2 | 1.1 | -0.30 | 0.17 |
| **4** | 183 | 3.8 | 6.4 | 0.1 | 1.0 | 1.1 | -0.04 | 0.14 |
| **5** | 151 | 4.7 | 5.6 | -0.1 | 1.1 | 1.1 | 0.05 | 0.00 |
| **6** | 121 | 5.4 | 4.9 | 0.4 | 0.9 | 1.1 | 0.01 | 0.21 |
| **7** | 85 | 7.9 | 1.7 | 3.9 | 1.0 | 0.9 | -0.02 | -0.12 |
| **8** | 76 | 5.1 | 0.6 | 3.2 | 0.6 | 0.7 | 0.05 | 0.08 |
| **9** | 78 | 8.6 | 1.6 | 5.2 | 1.1 | 0.9 | -0.02 | -0.20 |
| **10** | 55 | 15.6 | 1.7 | 5.6 | 1.3 | 1.0 | -0.11 | -0.17 |
| **11** | 76 | 14.5 | 2.6 | 6.1 | 1.8 | 1.1 | -0.21 | -0.49 |
| **12** | 66 | 15.8 | 3.5 | 2.0 | 1.7 | 1.2 | 0.07 | -0.53 |

Variables are described in the text.

analyzed, from ½ to 2 times the local ice thickness, we confirmed that localized variations in slope, ice thickness, and surface strain rates did not compromise our results. We report only the results that were invariant over this range of radii.

(3) A third problem is that we do not know the most appropriate value to use for the parameter $A$ in equation (8). Values for $A$ obtained by field studies of other temperate glaciers range from about $2 \times 10^{-24}$ to $6 \times 10^{-24}$ $\mathrm{Pa^{-3}s^{-1}}$ (Raymond, 1980; Hubbard and others, 1998), with a mean value for whole-glacier studies of $2.4 \times 10^{-24}$ $\mathrm{Pa^{-3}s^{-1}}$ (Cuffey and Paterson, 2010, p. 73). (The true value may vary within the glacier because of differences in water content or crystal c-axis fabrics.) The lower the value of $A$ used, the lower the calculated contribution of internal deformation to surface speed (eqs 2 and 3), and the larger the inferred rate of sliding (eq 1). Thus the maximum plausible value for $A$ is the one that gives $u_b = 0$. At our study site, we find that a value $A \approx 1.5 \times 10^{-24}$ $\mathrm{Pa^{-3}s^{-1}}$ gives $u_b = 0$ in the central part of the glacier. Because this maximal estimate roughly corresponds to the minimum of the range found at other temperate glaciers, we take it to be the most likely value.

For this value ($A = 1.5 \times 10^{-24}$ $\mathrm{Pa^{-3}s^{-1}}$), table 1 lists our inferred basal sliding speeds and force terms for the 12 cylindrical regions drawn on figure 7. The magnitude of basal drag is everywhere close to $10^5$ Pa, a typical result for mountain glaciers. Furthermore, the spatial variation in basal drag is less than that in the driving stress. Individually, the wall and longitudinal terms are locally significant but have no consistent influence on ice in the center of the cirque. Longitudinal force holds back the frontal ice (regions 7, 9–12) but pushes the ice forward at some upglacier sites (regions 1–4). Parts of the glacier are restrained by wall drag (regions 3 and 11) but, in contrast to the situation in a valley glacier (for example, Raymond, 1980), the wall drags have no consistent influence on the glacier center (regions 4, 5, 6). At regions 1 and 2, where one might expect wall drags to be significant, across-glacier variations in

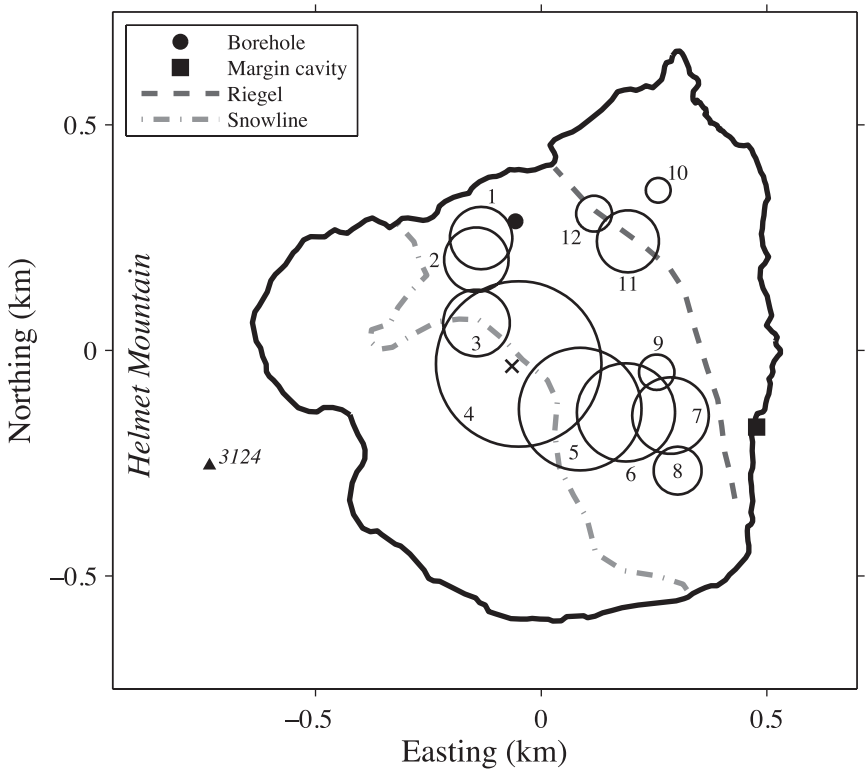


Fig. 7. Locations and surface areas of 12 cylindrical regions used for force balance and sliding calculations. Stress magnitudes and sliding rates are listed in table 1. Direct measurements of sliding rate were made in the borehole and margin cavity indicated.

ice thickness act to balance the across-glacier velocity gradient and reduce the retarding effect of the walls.

Inferred basal velocities vary from place to place, with sliding fractions (sliding rate divided by surface speed) ranging from 0 to 0.8; sliding motion appears to be negligible for the thick ice in the cirque basin, but speeds up toward the sides and, especially, over the riegel. Although the absolute values for sliding rates depend on several major assumptions, we have found that this spatial pattern is invariant with regard to all uncertainties. Unfortunately, we have not been able to expand this analysis to include much of the accumulation zone of WWG. The problem is that we do not know the density-depth profile of the thick firn around the headwalls, and therefore do not know the driving stress to sufficient accuracy. We have measured very high rates of vertical subsidence at the surface of the firn aprons, rates that can only be explained by compaction of a thick column of underlying material. Using a density for fully-formed ice in a force-balance analysis leads to calculated sliding rates near the headwall of about −10 m/yr, a physically implausible result.

### *Sliding Measured in a Borehole and a Frontal Cavity*

By observing the total annual displacement of painted ice and rocks on the roof of a large cavity for two years (fig. 8), we directly determined a sliding rate of 4.6 ± 0.2 m/yr at one site along the glacier terminus (location indicated by a square in figs. 5 and 7). We also obtained repeat inclinometry surveys in one uncased borehole near

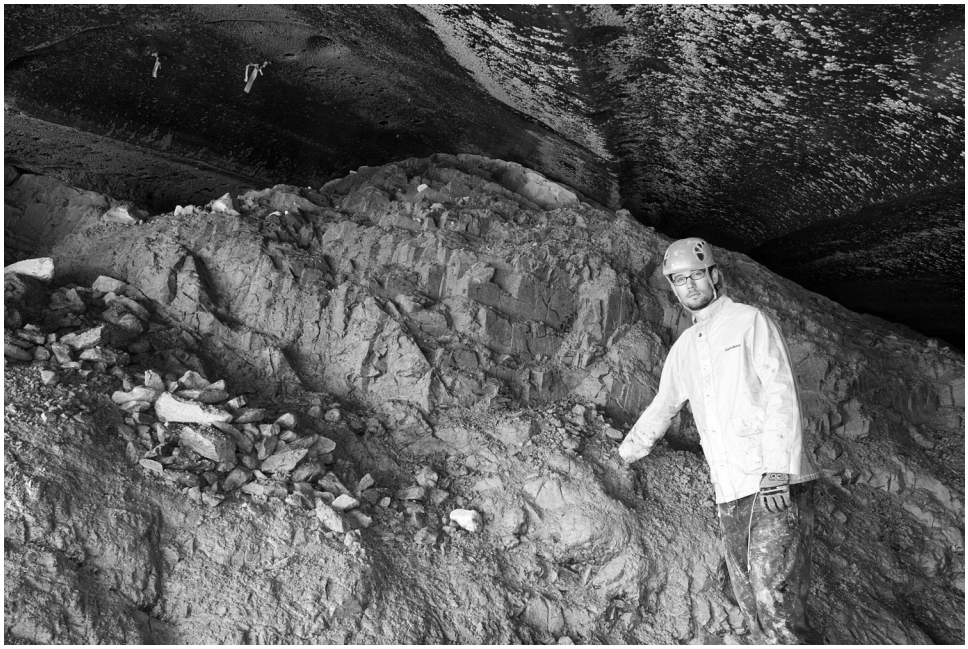

Fig. 8. Photograph looking upglacier from within the margin cavity. The cavity roof is the basal ice of the glacier. Ice screws (top-left) were used to monitor sliding during the summer field season; a strip of orange spray-paint applied directly to the basal ice recorded annual motion (4.6 ± 0.2 m/yr). Ice motion is out of the page.

the northern margin (location indicated by a filled circle in figs. 5 and 7). The borehole was drilled by a high-pressure jet of hot water. A steel wire frozen in the original borehole guided the drill during the reaming process for the repeat survey (boreholes in temperate glaciers freeze shut over time because of the reduced pressure or impurity content in them compared to the surrounding ice). We measured the three-dimensional shape of the initial and repeat boreholes using an Icefield Tools™ MI3 Multishot inclinometer. We recorded inclination and orientation at 2 m increments from the surface to the bed by lowering the inclinometer with a static rope. Each borehole was surveyed twice and then averaged; we used the variance between same-year surveys to estimate error magnitudes. The inclinometry analysis indicated annual sliding of 1.6 ± 0.3 m/yr (about 50% of the surface motion) at the borehole (fig. 9). For the same region of the glacier (cylinders 1 and 12 upstream and downstream of the borehole, respectively), our force balance analysis suggested sliding rates of 2.7 and 2.0 m/yr, or about 70 percent and 40 percent of the surface motion. The qualitative agreement with the nearby borehole measurements is encouraging. We were not able to calculate a force balance at the borehole itself because we had no measurements of the transverse strain rate on its north side. (We did drill boreholes closer to the glacier center and within our survey grid. Unfortunately, we were unable to perform repeat borehole inclinometry due to the cool weather and resulting lack of surface water to use in the drill system).

### *Robustness of Force Balance Modeling and Calculated Sliding Rates*

Qualitative features of our inferred patterns of sliding rate and force partitioning are robust. As noted previously, even with an exceptionally low value for the creep

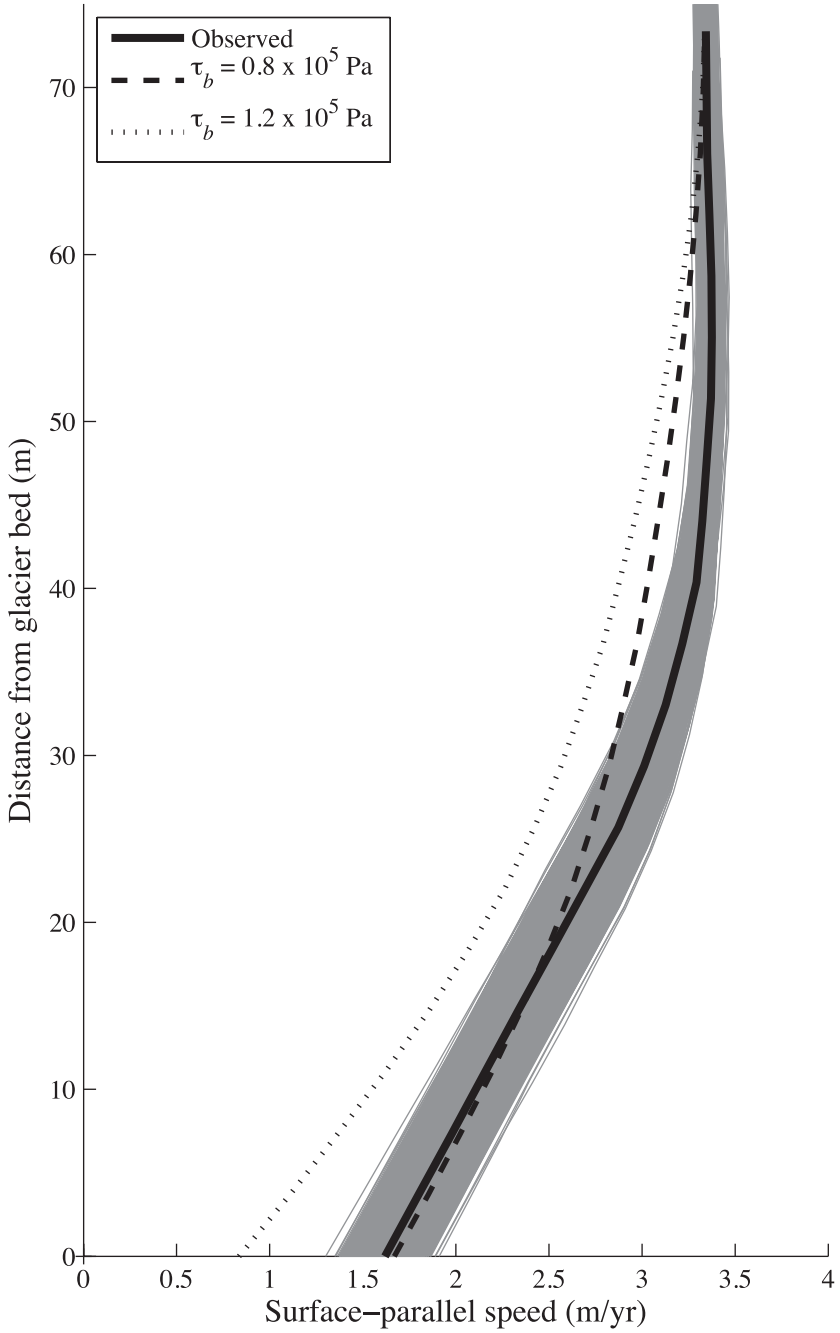


Fig. 9. Repeat borehole inclinometry deformation profile (between 8/15/2007 and 8/16/2008) of a single borehole (total depth = 73.4 m; solid black circle in figs. 5 and 7). Gray lines represent deformation profiles for 1500 Monte-Carlo simulations that incorporated both instrumental and measurement errors. Internal deformation accounts for about 50% of the total surface motion. For comparison, we also present two modeled profiles using basal shear stress values found at regions 1 and 12 (bounding the borehole) and $A = 1.5 \times 10^{-24}\,\mathrm{Pa}^{-3}\mathrm{s}^{-1}$.

parameter *A*, the classical slab glacier theory (Nye, 1952) predicts a shear velocity similar to measured surface velocity in the cirque center (region 4 of fig. 7). Here, basal motion must be a minor component of the total, given the small magnitude of strain-rate gradients in the surrounding region. In contrast, basal motion is required to explain observed velocities in thinner ice regions over the riegel and near the margins. Indeed, measurements of sliding in a borehole and in a marginal cavity (in different regions of the glacier) both qualitatively agree with our more detailed calculations. A Monte-Carlo analysis provides a quantitative assessment of the sensitivity of our results to primary uncertainties. Figure 10 compares calculated sliding rates and basal drags for two locations, one centered above the overdeepening and one on the riegel. Figure 11 shows the error-induced variability in stress terms (eq 7) used to calculate basal shear stress at region 7 (fig. 10). These distributions show the implications of all uncertainties in field measurements and of the different assumptions about variations of strain rates with depth. The discrimination between comparatively slow and fast sliding sites is moderately strong. The non-linear properties of ice deformation lead to a broad range of solutions, so the discrimination is not perfect.

## DISCUSSION

The cirque glacier cannot be regarded as a rigid body. Temperate ice deforms significantly at a deviatoric stress of $10^5$ Pa; in simple shear, for example, $10^5$ Pa of stress implies a velocity gradient of at least 0.1 per year. Because the basal drag of WWG is close to $10^5$ Pa, and because the glacier flows slowly despite a thickness of as much as 185 m, internal shearing must account for a significant fraction of the glacier's motion. This claim is confirmed by our analysis of observed surface velocities and measurements in one borehole. "Internal shearing" in this case refers to the dominant bed-parallel component. Ice deformations of other orientations modulate the glacier's dynamics through "stress-gradient coupling" of the flow (Nye, 1957; Kamb and Echelmeyer, 1986). As the values in table 1 show, the spatial variations of basal drag are subdued compared to those of driving stress; as in larger glaciers, the wall and longitudinal forces act to spatially average the driving stress, reducing variations of basal drag. Transverse and longitudinal strain rates at the surface of WWG, calculated from the velocity field shown in figure 5, range from $-4.8\times10^{-2}$/yr to $+5.7\times10^{-2}$/yr and $-6.3\times10^{-2}$/yr to $+7.9\times10^{-2}$/yr, respectively. In general, the transverse and longitudinal straining describe a rather irregular pattern, related to local-scale variations of basal topography, ice thickness, and surface slope. Some of these variations, in turn, reflect the presence of two headwalls (one western and one southern), the division of the western headwall into two alcoves, and the riegel and its partial breach.

In some respects, our study site confirms that a cirque glacier's "unusual bed configuration" makes its flow "rather different from other glacier types" (Summerfield, 1991, p. 274). As figure 6 illustrates, the flux along a flowline reaches a maximum in the middle of the glacier, a consequence of the distribution of accumulation and ablation. This is the typical pattern for land-terminating mountain glaciers. In such typical glaciers, however, the increase of flux is accommodated primarily by a downglacier increase of velocity (longitudinal extension) in the accumulation zone, and by a decrease of velocity in the ablation zone. In WWG, by contrast, the increase of flux is largely accommodated by increased ice thickness in the center of the cirque basin. Thus, although ice in WWG strains longitudinally, such deformations are less significant than in a typical valley glacier; the pattern in WWG defines a rotation that conforms with the concave bed. Another unusual aspect of WWG in its present configuration depends on the riegel. Because the ice thins rapidly from the middle of the cirque onto the crest of the riegel, a large part of WWG's ablation zone undergoes longitudinal extension rather than compression, at least in the upper layers. To drive flow over the riegel, the glacier surface must steepen. Over the deep cirque center, in

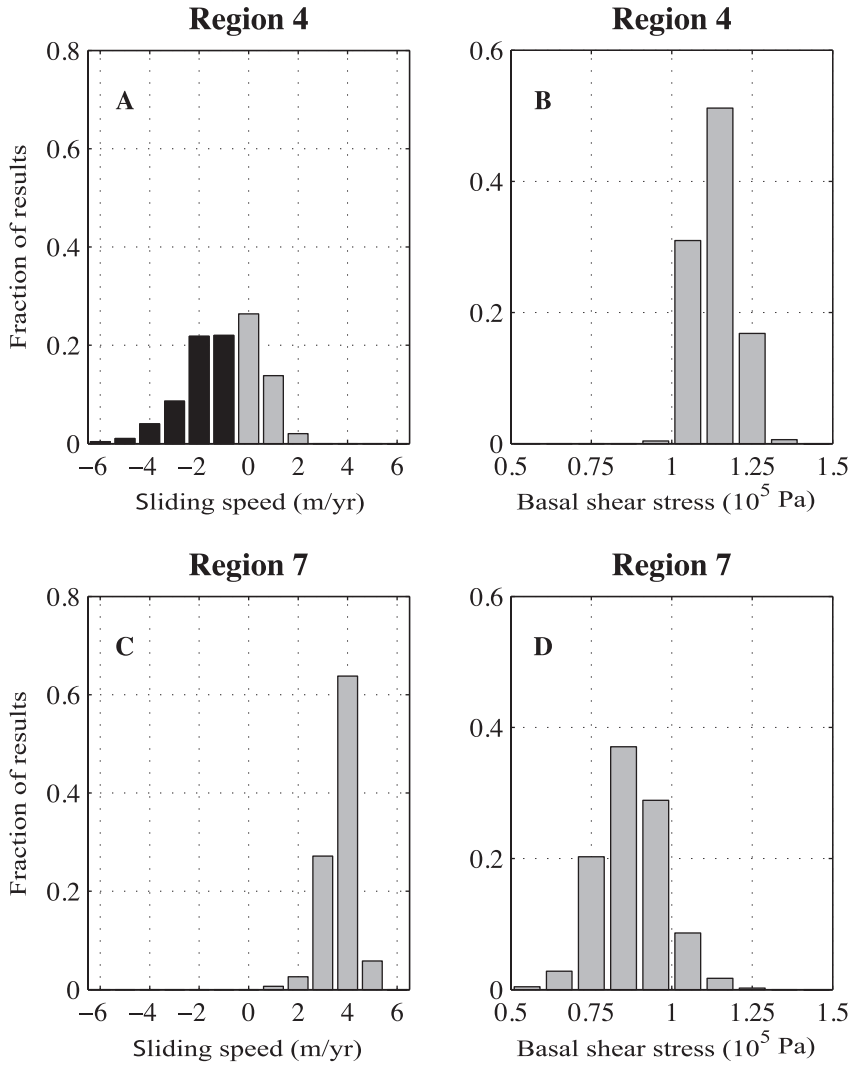


Fig. 10. Monte-Carlo results for (A, B) a slow-sliding region (cylinder 4 of fig. 7) and (C, D) a fast-sliding region (cylinder 7 of fig. 7). Each bin height represents the fraction of simulations that give results within the bin interval. At region 4, 84% of simulations produce sliding rates less than 1 m/yr (median = −0.8 m/yr). At region 7, 97% of simulations produce sliding rates greater than 2 m/yr (median = 3.7 m/yr). Basal shear stress in the glacier's center is best constrained because ice thickness measurements are most accurate away from the margins, and longitudinal stress terms are negligible there. Negative sliding rates (shown in black) are physically implausible, but decreasing the parameter $A$ would shift the sliding rate distributions to higher values.

contrast, the surface is nearly flat; the riegel acts like a dam. (Note that, consistent with the dam analogy, the riegel restrains the glacier not through an along-flow gradient of longitudinal compression (regions 4 and 5 in table 1) but by flattening the surface upstream and so limiting the driving stress.) Furthermore, because of the near-level surface in the cirque center, the driving stress on a profile drawn across-glacier does not reach a pronounced maximum in the center, as it would in a valley glacier. Thus, in comparison to a valley glacier, the across-glacier variation of velocity is muted.

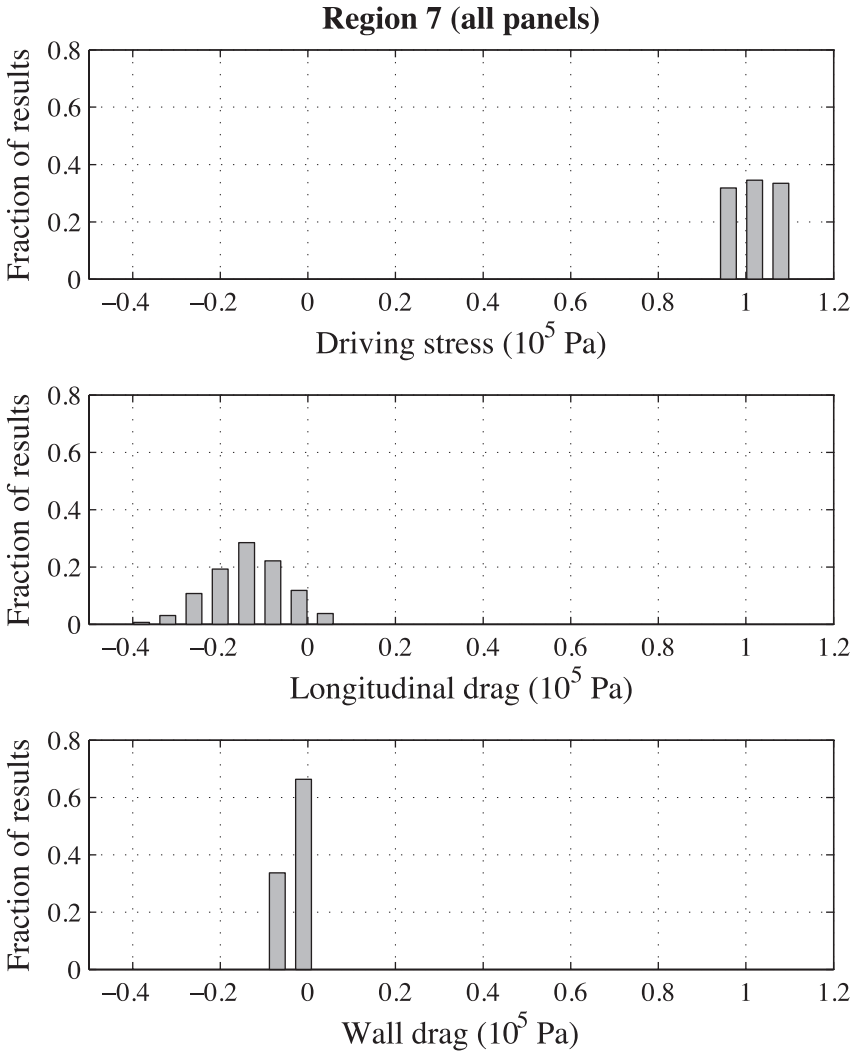


Fig. 11. Monte-Carlo results for stress magnitudes ($\tau_d$, $\tau_l$, and $\tau_w$, respectively) at region 7 in fig. 7. At this location, the longitudinal drag term shows the highest variability and contributes the largest uncertainties to our inferred basal sliding rates.

The paramount geomorphological question, however, is not how the glacier deforms and rotates internally but how the rate of basal slip varies spatially (Hallet, 1979 and 1996; Oerlemans, 1984; Harbor and others, 1988; MacGregor and others, 2000). Our analyses demonstrate that slip is minimum in the middle of the cirque (with a value most likely about zero) and increases toward the lateral shear margins and onto the riegel. Thus the flow of WWG follows a pattern inferred elsewhere in larger temperate mountain glaciers (for example, the pattern of Nigardsbreen, Norway, inferred by Oerlemans, 1997). Given a magnitude of basal drag, the contribution of internal shearing to a glacier's surface velocity increases directly with the ice thickness, whereas the contribution from basal slip does not. To accommodate a given ice flux, the rate of slip must therefore tend to increase in regions of thin ice, such as

ice falls and riegels. If the erosion rate increases as a function of basal slip rate (Boulton, 1974; Hallet, 1979 and 1996; Oerlemans, 1984; Amundson and Iverson, 2006; MacGregor and others, 2009), then WWG is currently scouring its riegel and northern marginal wall, but not its central basin. In essence, the riegel interferes with the flow and is therefore being ground down. If persistent over time, such a pattern would destroy the archetypal cirque morphology. The same pattern likely applies during colder climates, when the cirque sits at the head of a much longer glacier. In such a situation, the entire cirque is in the accumulation zone and the ice flux must increase across the riegel, accentuating the downglacier increase of velocity.

How then does a cirque basin persist? Our results contradict the hypothesis that the overdeepening is amplified by enhanced sliding or maintained by rotational sliding. Some models of glacial erosion assume a correlation between ice flux and erosion rate, and some analyses of landforms support this assumption (Amundson and Iverson, 2006; Anderson and others, 2006). Indeed the ice flux at WWG reaches a maximum in the cirque center (fig. 6A). This is not relevant, however, because ice flux only enters the assumed erosion relations as a proxy for sliding rate. At WWG, ice flux and sliding rate do not appear to correlate. Several alternatives discussed by earlier investigators remain viable. One possibility is that the pattern of erosion rate depends overwhelmingly on hydrological factors such as temporal variability of subglacial water pressure (Hooke, 1991; Iverson, 1991; Hallet, 1996; Cohen and others, 2006). Basal freeze-on of supercooled water might suppress erosion on the upglacier side of the riegel (Alley and others, 2003), but only after the basin is fully formed (the upglacier bed slope must exceed a critical value for supercooling to occur). At WWG, in fact, the geometry is conducive to freeze-on above the riegel, but measurements suggest that water temperatures are too high for freezing at present (Dow, ms, 2009). A second possibility is that cirque glaciers accomplish significant erosion only in periods of comparatively warm climates, when the glaciers are small and terminate on the upvalley side of the riegel or in the basin (MacGregor and others, 2009). Small cirque glaciers can survive in comparatively warm climates—when ice has disappeared from the rest of the landscape—because the headwalls shade the glacier surface and focus accumulation by avalanching (Graf, 1976; DeBeer and Sharp, 2009).

As a final note, we are mindful that our study evaluates the behavior of a cirque glacier at one moment in time. The magnitude of basal sliding beneath past or future versions of WWG remains an unknown. A simple calculation, however, provides some insight. Using trimlines and historical photos, we estimate that WWG was roughly 30 and 80 meters thicker during the Little Ice Age and Last Glacial Maximum, respectively. Given that basal shear stresses would have remained about $10^5$ Pa, the thicker glacier would have transmitted more ice (per unit width) by deformation. Our thickness estimates imply that deformational fluxes increased by a factor of 1.35 and 2, relative to the present-day. Are these past deformational fluxes large enough to transmit the increase in accumulation that occurred in colder climates without requiring a component of sliding? For a basal shear stress of $10^5$ Pa, deformation alone can accommodate upglacier snowfall rates from about 4 to 6 m/yr during the Last Glacial Maximum and about 2.5 to 4 m/yr during the Little Ice Age. These values suggest that, even if present-day snowfall rates (3–5 m/yr) are maintained in colder climates and *no* ablation occurs within the cirque, basal sliding within the overdeepening was minimal even during recent glacial periods.

## CONCLUSION

We have investigated the flow of a small temperate glacier occupying an alpine cirque of archetypal form. The glacier does not conform to the classic rigid rotation model, a model that is often assumed but that has never been tested by modern glaciological analysis. Partitioning between internal deformation and basal slip varies

significantly from place to place on the glacier. Basal slip is at a minimum in the center of the cirque basin, where the rate is most likely near zero. The glacier behaves in many respects like an ordinary mountain glacier, with basal drags close to $10^5$ Pa and reduced spatial variations of flow because of transverse and longitudinal deformations. The glacier does, however, rotate to conform with the basin topography, but the rotation is achieved by internal deformation (including firn compaction). If erosion increases with sliding velocity, then, at present, the glacier is excavating the flanks of its basin and wearing down the riegel at its downvalley edge, a pattern that implies a damping of the archetypal cirque morphology.

ACKNOWLEDGMENTS

The authors wish to thank Jeffrey Moore, Jenny Cooper, Mary Dain, Luke Sanders, Dom Galic, Tom Tobin, Sabrina Belknap, Elena Evans, Ian Nicholson, Andrew Bliss, Yosuke Adachi and Justin Beckers for invaluable assistance in the field. Don McTighe, Craig Ward and Paul Quanstrom of Alpine Helicopters™ provided expertise and help far beyond their call of duty. We are grateful to Richard Alley, Robert Anderson, Ian Evans and an anonymous reviewer for perceptive and thorough reviews. This report is based on work funded by NSF grant EAR-0518608 to KMC, grant EAR-0517967 to KRM, a NSERC Discovery grant to JLK, and an Alberta Ingenuity Graduate Scholarship to CFD. We thank Michael Ellis and the Geomorphology and Land-Use Dynamics program at the NSF for partial support of this project.

## References

Alley, R. B., Lawson, D. E., Larson, G. J., Evenson, E. B., and Baker, G. S., 2003, Stabilizing feedbacks in glacier-bed erosion: Nature, v. 424, p. 758–760, doi: 10.1038/nature01839.

Amundson, J. M., and Iverson, N. R., 2006, Testing a glacial erosion rule using hang heights of hanging valleys, Jasper National Park, Alberta, Canada: Journal of Geophysical Research, v. 111, F01020, doi: 10.1029/2005JF000359.

Anderson, R. S., Molnar, P., and Kessler, M. A., 2006, Features of glacial valley profiles simply explained: Journal of Geophysical Research, v. 111, F01004, doi: 10.1029/2005JF000344.

Bahr, D. B., Pfeffer, W. T., and Meier, M. F., 1994, Theoretical limitations to englacial velocity calculations: Journal of Glaciology, v. 40, p. 509–518.

Boulton, G. S., 1974, Processes and patterns of glacial erosion, *in* Coates, D. R., editor, Glacial Geomorphology: Binghamton, State University of New York, p. 41–87.

Brocklehurst, S. H., and Whipple, K. X., 2002, Glacial erosion and relief production in the Eastern Sierra Nevada, California: Geomorphology, v. 42, n. 1–2, p. 1–24, doi: 10.1016/S0169-555X(01)00069-1.

Brook, M. S., Kirkbride, M. P., and Brock, B. W., 2006, Cirque development in a steadily uplifting range: rates of erosion and long-term morphometric change in alpine cirques in the Ben Ohau Range, New Zealand: Earth Surface Processes and Landforms, v. 31, p. 1167–1175, doi: 10.1002/esp.1327.

Clark, J. M., and Lewis, W. V., 1951, Rotational movement in cirque and valley glaciers: Journal of Geology, v. 59, p. 546–566, doi: 10.1086/625911.

Cohen, D., Hooyer, T. S., Iverson, N. R., Thomason, J. F., and Jackson, M., 2006, Role of transient water pressure in quarrying: A subglacial experiment using acoustic emissions: Journal of Geophysical Research, v. 111, F03006, doi: 10.1029/2005JF000439.

Cook, D. G., 1975, Structural style influenced by lithofacies, Rocky Mountain Main Ranges, Alberta-British Columbia: Geological Survey of Canada Bulletin, v. 233, p. 1–73.

Cuffey, K. M., and Paterson, W. S. B., 2010, The Physics of Glaciers (Fourth edition): Boston, Elsevier, 693 p.

Daly, R. A., 1905, The accordance of summit levels among alpine mountains: the fact and its significance: Journal of Geology, v. 13, p. 105–125, doi: 10.1086/621212.

Davis, W. M., 1906, The sculpture of mountains by glaciers: Scottish Geographical Magazine, v. 22, p. 76–89, doi: 10.1080/00369220608733647.

DeBeer, C. M., and Sharp, M. J., 2009, Topographic influences on recent changes of very small glaciers in the Monashee Mountains, British Columbia, Canada: Journal of Glaciology, v. 55, n. 192, p. 691–700, doi: 10.3189/002214309789470851.

Dow, C. F., ms, 2009, Subsurface hydrological characteristics of an overdeepened cirque glacier: Edmonton, Alberta, University of Alberta, Masters thesis, 152 p.

Evans, I. S., 1997, Process and form in the erosion of glaciated mountains, *in* Stoddart, D. R. editor, Process and Form in Geomorphology: London, Routledge, p. 145–174.

——— 2006, Glacial landforms, erosional features: major scale forms, *in* Elias, S. A., editor, Encyclopedia of Quaternary Science: Elsevier, Amsterdam, v. 1, p. 838–852, doi: 10.1016/B0-44-452747-8/00098-3.

Foster, D., Brocklehurst, S. H., and Gawthorpe, R. L., 2008, Small valley glaciers and the effectiveness of the glacial buzzsaw in the northern Basin and Range, USA: Geomorphology, v. 102, p. 624–639, doi: 10.1016/j.geomorph.2008.06.009.

Gastaldi, S. B., 1873, On the effects of glacier-erosion in Alpine valleys: Quarterly Journal of the Geological Society, v. 29, n. 1–2, p. 396–401, doi: 10.1144/GSL.JGS.1873.029.01-02.30.

Gibson, G. R., and Dyson, J. L., 1939, Grinnell Glacier, Glacier National Park, Montana: Geological Society of America Bulletin, v. 50, p. 681–696.

Graf, W. L., 1976, Cirques as glacier locations: Arctic and Alpine Research, v. 8, n. 1, p. 79–90, doi: 10.2307/1550611.

Hallet, B., 1979, A theoretical model of glacial abrasion: Journal of Glaciology, v. 23, n. 89, p. 39–50.

——— 1996, Glacial quarrying: a simple theoretical model: Annals of Glaciology, v. 22, p. 1–8.

Harbor, J. M., Hallet, B., and Raymond, C. F., 1988, A numerical model of landform development by glacial erosion: Nature, v. 333, p. 347–349, doi: 10.1038/333347a0.

Helland, A., 1877, On the ice-fjords of North Greenland and on the formation of fjords, lakes, and cirques in Norway and Greenland: Quarterly Journal of the Geologic Society, London, v. 33, p. 142–176, doi: 10.1144/GSL.JGS.1877.033.01-04.10.

Hooke, R. LeB., 1991, Positive feedbacks associated with erosion of glacial cirques and overdeepenings: Geological Society of America Bulletin, v. 103, p. 1104–1108, doi: 10.1130/0016-7606(1991)103<1104:PFAWEO>2.3.CO;2.

Hubbard, A., Blatter, H., Nienow, P., Mair, D., and Hubbard, B., 1998, Comparison of a three-dimensional model for glacier flow with field data from Haut Glacier d'Arolla, Switzerland: Journal of Glaciology, v. 44, p. 368–378.

Iverson, N. R., 1991, Potential effects of subglacial water-pressure fluctuations on quarrying: Journal of Glaciology, v. 37, p. 27–36.

Johnson, W. D., 1904, The profile of maturity in alpine glacial erosion: Journal of Geology, v. 12, n. 7, p. 569–578, doi: 10.1086/621181.

Kamb, B., and Echelmeyer, K. A., 1986, Stress-gradient coupling in glacier flow: 1. Longitudinal averaging of the influence of ice thickness and surface slope: Journal of Glaciology, v. 32, p. 267–284.

Kavanaugh, J. L., and Cuffey, K. M., 2009, Dynamics and mass balance of Taylor Glacier, Antarctica: 2. Force balance and longitudinal coupling: Journal of Geophysical Research, v. 114, F04011, doi: 10.1029/2009JF001329.

Lawson, A. C., 1904, The geomorphogeny of the Upper Kern Basin: University of California Publications, Bulletin of the Department of Geology, v. 3, n. 15, p. 291–376.

Lewis, W. V., 1960, The problem of cirque erosion, *in* Lewis, W. V., editor, Norwegian Cirque Glaciers: Royal Geographical Society Research Series, v. 4, p. 97–100.

Luckman, B. H., and Osborn, G. D., 1979, Holocene glacier fluctuations in the Middle Canadian Rocky Mountains: Quaternary Research, v. 11, p. 52–77, doi: 10.1016/0033-5894(79)90069-3.

MacGregor, K. R., Anderson, R. S., Anderson, S. P., and Waddington, E. D., 2000, Numerical simulations of glacial-valley longitudinal profile evolution: Geology, v. 28, n. 11, p. 1031–1034, doi: 10.1130/0091-7613(2000)28<1031:NSOGLP>2.0.CO;2.

MacGregor, K. R., Anderson, R. S., and Waddington, E. D., 2009, Numerical modeling of glacial erosion and headwall processes in alpine valleys: Geomorphology, v. 103, p. 189–204, doi: 10.1016/j.geomorph.2008.04.022.

Matthes, F. E., 1900, Glacial sculpture of the Bighorn Mountains, Wyoming: United States Geological Survey Annual Report, v. 21, p. 167–190.

Maxwell, D., Truffer, M., Avdonin, S., and Stuefer, M., 2008, An iterative scheme for determining glacier velocities and stresses: Journal of Glaciology, v. 54, p. 888–898.

McCall, J. G., 1952, The internal structure of a cirque glacier: report on studies of the englacial movements and temperatures: Journal of Glaciology, v. 2, p. 122–131.

——— 1960, The flow characteristics of a cirque glacier and their effect on glacial structure and cirque formation, *in* Lewis, W. V., editor, Norwegian Cirque Glaciers: The Royal Geographical Society Research Series, v. 4, p. 39–62.

McLaren, P., and Hills, L. V., 1973, Cirque analysis as a method of predicting the extent of a Pleistocene ice advance: Canadian Journal of Earth Sciences, v. 10, p. 1211–1225.

Mitchell, S. G., and Montgomery, D. R., 2006, Influence of a glacial buzzsaw on the height and morphology of the Cascade Range in central Washington State, USA: Quaternary Research, v. 65, p. 96–107, doi: 10.1016/j.yqres.2005.08.018.

Naylor, S., and Gabet, E. J., 2007, Valley asymmetry and glacial versus nonglacial erosion in the Bitterroot Range, Montana, USA: Geology, v. 35, p. 375–378, doi: 10.1130/G23283A.1.

Nye, J. F., 1952, The mechanics of glacier flow: Journal of Glaciology, v. 2, p. 82–93.

——— 1957, The distribution of stress and velocity in glaciers and ice-sheets: Proceedings of the Royal Society of London, Series A, v. 239, p. 113–133, doi: 10.1098/rspa.1957.0026.

Oerlemans, J., 1984, Numerical experiments on large-scale glacial erosion: Zeitschrift für Gletscherkunde und Glazialgeologie, v. 20, p. 107–126.

——— 1997, A flowline model of Nigardsbreen, Norway: projection of future glacier length based on dynamic calibration with the historic record: Annals of Glaciology, v. 24, p. 382–389.

Oskin, M., and Burbank, D. W., 2005, Alpine landscape evolution dominated by cirque retreat: Geology, v. 33, p. 933–936, doi: 10.1130/G21957.1.

Penck, A., 1905, Glacial features in the surface of the Alps: The Journal of Geology, v. 13, n. 1, p. 1–19, doi: 10.1086/621202.

Raymond, C. F., 1980, Temperate valley glaciers, *in* Colbeck, S. C., editor, Dynamics of Snow and Ice Masses: New York, Academic Press, p. 79–139.

Richter, E., 1900, Geomorphologische untersuchungen in den Hochalpen: Petermann's Geographische Mitteilungen, v. 29, p. 1–103.
Ritter, D. F., Kochel, R. C., and Miller, J. R., 2002, Process Geomorphology (Fourth Edition): New York, McGraw-Hill, 560 p.
Summerfield, M. A., 1991, Global Geomorphology: Essex, Longman Scientific and Technical, 537 p.
Trenhaile, A. S., 1976, Cirque morphometry in the Canadian Cordillera: Annals of the Association of American Geographers, v. 66, n. 3, p. 451–462, doi: 10.1111/j.1467-8306.1976.tb01101.x.
Truffer, M., 2004, The basal speed of valley glaciers: an inverse approach: Journal of Glaciology, v. 50, p. 236–242 doi: 10.3189/172756504781830088.
van der Veen, C. J., and Whillans, I. M., 1989, Force budget. 1. Theory and numerical methods: Journal of Glaciology, v. 35, p. 53–60.
Waldrop, H. A., 1964, Arapaho Glacier: a sixty-year record: University of Colorado Studies, Geology Series, v. 3, 37 p.
Weertman, J., 1971, Shear stress at the base of a rigidly rotating cirque glacier: Journal of Glaciology, v. 10, n. 58, p. 31–37.